Journal of Non-Crystalline Solids 358 (2012) 1818–1829

Contents lists available at SciVerse ScienceDirect

Journal of Non-Crystalline Solids

journal homepage: www.elsevier.com/ locate/ jnoncrysol

# Effect of glass composition on activation energy of viscosity in glass-melting-temperature range

Pavel Hrma [a,b,*], Sang-Soo Han [a]

[a] Division of Advanced Nuclear Engineering, Pohang University of Science and Technology, Pohang, Republic of Korea
[b] Pacific Northwest National Laboratory, Richland, WA 99352, USA

ARTICLE INFO

*Article history:*
Received 7 February 2012
Received in revised form 14 May 2012
Available online 10 June 2012

*Keywords:*
Glass viscosity;
Nuclear waste glass;
Viscosity–composition relationship;
Activation energy;
Mixture models

ABSTRACT

In the high-temperature range, where the viscosity ($\eta$) of molten glass is $<10^3$ Pa s, the activation energy ($B$) is virtually independent of temperature ($T$). Moreover, the coefficient $A$ in the Arrhenius relationship, $\ln(\eta) = A + B/T$, is nearly independent of melt composition. Hence, the viscosity–composition relationship for $\eta < 10^3$ Pa s is defined by $B$ as a function of composition. Using a database encompassing over 1300 compositions of high-level waste glasses with nearly 7000 viscosity data, we developed mathematical models for $B(\mathbf{x})$, where $\mathbf{x}$ is the composition vector in terms of mass fractions of components. In this paper, we present 13 versions of $B(\mathbf{x})$ as first- and second-order polynomials with coefficients for 15 to 39 components, including *Others*, a component that sums constituents having little effect on viscosity.



## 1. Introduction

Under normal conditions, glass viscosity ($\eta$) is a function of temperature ($T$) and composition, i.e., $\eta = \eta(T,\mathbf{x})$, where $\mathbf{x}$ is the composition vector (array of mass or mole fractions of glass components). Historically, viscosity–composition relationships were mostly restricted to tables and diagrams [1–3], although various formulas were proposed for limited composition regions. Only when large databases, such as SciGlass [3], became available in electronic form, did serious attempts begin to reduce large amounts of data to coefficients of polynomial functions of mass or mole fractions of components [4]. Such functions are often constructed in terms of isokoms, i.e., $T = f_\eta(\mathbf{x})$, that relate the temperature to composition with $\eta$ as a parameter. The isokom representation leaves to the user the choice of the form of $\eta = f_\mathbf{x}(T)$, i.e., the viscosity–temperature function for a given composition, from among dozens of relationships; among these, the Vogel–Fulcher–Tammann equation and the Adams-Gibbs equation are the most popular (some authors fit both these equations to their data [5]). However, the freedom to select an appropriate $\eta = f_\mathbf{x}(T)$ function from the smorgasbord of available choices is limited by the number of parameters of the $T = f_\eta(\mathbf{x})$ relation, which is usually small—typically just three. On the other hand, the number of $\eta(T)$ data for glasses is usually large enough to enable a satisfactory choice of a representative approximation function. Alternatively, viscosity can be expressed as $\eta = f_T(\mathbf{x})$, where $T$ is the parameter. Therefore, it is advantageous to preselect an analytical form of $\eta = f_\mathbf{x}(T)$ and then express its coefficients as functions of composition [6–8].

The task of selecting an adequate $\eta = f_\mathbf{x}(T)$ function for a family of glasses, such as borosilicate commercial glasses or nuclear waste glasses, can be facilitated by the following assumptions [8] that rule out many, if not most, $\eta = f_\mathbf{x}(T)$ relationships proposed in the literature:

1. The viscosity at the glass transition temperature, $T_g$, is independent of composition.
2. As $T$ increases, the $\eta = f_\mathbf{x}(T)$ function asymptotically approaches the Arrhenius function, $\ln(\eta) = A + B/T$, with the coefficient $A$ independent of composition.
3. The $\eta = f_\mathbf{x}(T)$ function approaches the Arrhenius function fast enough to become virtually indistinguishable from it (within experimental error) when the viscosity is below $10^2$ to $10^3$ Pa s, depending on the glass family and measurement accuracy.
4. The number of temperature-independent coefficients should be as low as possible.

*Note*: Some authors postulate that $\eta \to \infty$ only when $T \to 0$ [9,10]. However, this condition has no practical implications in glass technology and its theoretical justification is arguable. It can be met either with more empirical coefficients [9] or by violating some of the constitutive assumptions stated above.

By assumptions 2 and 3, high-temperature viscosity data (i.e., $\eta < 10^3$ Pa s), both for commercial and waste glasses, are satisfactorily fitted by the Arrhenius function [6,7,11] with a temperature-independent activation energy ($B$),

$$\ln(\eta) = A + B(\mathbf{x})/T \tag{1}$$

* Corresponding author at: Pacific Northwest National Laboratory, Richland, WA 99352, USA.
*E-mail address:* pavelhrma@postech.ac.kr (P. Hrma).

0022-3093/$ – see front matter © 2012 Elsevier B.V. All rights reserved.
doi:10.1016/j.jnoncrysol.2012.05.030

where $A$ is a constant coefficient. This equation has a great advantage in its simplicity, having only two coefficients, $A$ and $B$, of which only $B$ depends on glass composition. Because viscosity is usually around 10 Pa s at glass-processing temperatures, it is suitable for formulating glasses that meet melt-processing constraints.

The activation energy is usually expressed as a function of composition using the concept of partial properties [11,12]. Thus,

$$B = \sum_{i=1}^{N} B_i x_i \tag{2}$$

where $x_i$ is the $i$th component's mass fraction, $B_i$ is the $i$th component's partial specific activation energy, and $N$ is the number of components.

Partial properties are themselves functions of composition, but $B_i$s can be approximated as constants for narrow ranges of mass fractions. For highly interactive components, especially those with a wide range of mass fractions, $B_i$s can be approximated as linear functions of composition. Thus,

$$B_i = \sum_{j=1}^{N} \bar{B}_{ij} x_j \tag{3}$$

where $\bar{B}_{ij}$ is the $i$th and $j$th components' second-order coefficient.

Combining Eqs. (2) and (3) and rearranging, we obtain

$$B = \sum_{i=j}^{N} \sum_{j=1}^{N} B_{ij} x_i x_j \tag{4}$$

where $B_{ii} = \bar{B}_{ii}$ and $B_{ij} = \bar{B}_{ij} + \bar{B}_{ji}$ (the $\bar{B}_{ij}$matrix is not necessarily symmetrical). Hence, the number of terms in Eq. (4) is $N_2 = (1/2)N(N+1)$, corresponding to $N_2$ second-order coefficients.

Compared to commercial glasses, high-level waste (HLW) glasses have a large number of components with concentrations not encountered in commercial industry or in geology. Developing mathematical models that relate viscosity to composition for these glasses is not only important for waste glass formulation, but also interesting to researchers who endeavor to relate empirical coefficients to the melt structure.

Obtaining second-order coefficients for a large number of components requires a large number of data. If each coefficient should be supported by at least 4 independent data points, 220 data points are needed for a mixture with just 10 components. Fortunately, a huge viscosity database has been accumulated for HLW glasses at various laboratories in the U.S. over the past decades. The database compiled at Pacific Northwest National Laboratory [13] comprises over 1300 compositions with 83 components and nearly 7000 data for viscosities $<10^3$ Pa s. The linear independence of the glass components was demonstrated by the scatter-plot matrix as well as the correlation matrix [13]. Using this database and Eqs. (1) to (4), we have developed several versions of viscosity–composition relationships with various solutions for first- and second-order coefficients.

Unlike viscosity–composition relationships based on limited numbers of glass compositions specifically tailored for the model development [7,11], or on a broad composition region available from the literature [4], we used a large amount of data collected from various sources, but confined to nuclear waste glasses [13]. The model previously developed from this database preferred the Vogel–Fulcher–Tammann equation fitted to 967 data points using 72 parameters and 23 components ($R^2 = 0.96$). Because viscosity data in this database are within the Arrhenius range of the $\eta = f_{\boldsymbol{x}}(T)$ relationships, assumptions 2 and 3 stated above allowed us to develop models based on Eq. (4) and representing 5900 to 6200 data with 25–60 parameters and up to 39 components ($R^2 = 0.98$). Model fitting was done with the solver of Excel. We have explored the effects of model design on the model applicability to glass formulation and on the response of melt viscosity to composition variability. Thus, apart from providing collections of ready-made coefficients for viscosity estimates, our work may open a discussion about the construction of the viscosity–composition relationships.

## 2. Data preparation

The Pacific Northwest National Laboratory (PNNL) database [13] reports both targeted and analytical compositions. Because analytical data were not obtained for a substantial number of glasses, we chose the targeted compositions for model development. Before fitting model equations to data, we have simplified the database using the redox state convention, restricting the composition region, and defining and imposing a data acceptability limit. These data arrangements are described below.

### 2.1. Redox state convention

Out of 83 components identified in the database, oxides of various elements (As, Ce, Co, Fe, Mn, Mo, Pb, Pr, Re, Rh, Sb, Sn, Tc, Tl, and U) are listed in more than one valence state in the database [13]. These valence states do not necessarily correspond to their actual presence in molten glass at the temperature of viscosity measurement. Therefore, we followed an established convention of choosing a single valency for each of these oxides: $As_2O_3$, $Ce_2O_3$, CoO, $Fe_2O_3$, MnO, $MoO_3$, PbO, $Pr_2O_3$, $Re_2O_7$, $Rh_2O_3$, $Sb_2O_3$, SnO, $Tc_2O_7$, $Tl_2O$, and $UO_2$. Even though oxides in different oxidation states affect viscosity differently, their proportions are neither arbitrary nor fully determined by the batch materials if we assume that the glasses were reasonably close to equilibrium with air or oxygen bubbles at some specific temperature. Thus, provided that the partial pressure of oxygen was similar in glasses of different compositions, each $B_i$ coefficient obtained for a single oxide effectively represents the true redox state of the element.

To make up for the changes in oxygen concentration caused by application of the redox state convention, we renormalized glass composition to component mass fractions that sum to 1, i.e.,

$$\sum_{i=1}^{N} x_i = 1 \tag{5}$$

On applying the single redox state convention, the number of components decreased to 56.

### 2.2. Minor components and $SO_3$

After sorting data by viscosity, we have removed from the database data with $\eta > 1050$ Pa s. This reduced the number of data points from 6884 to 6765. Then, using Eq. (1), we calculated the activation energy for each data point, i.e., each ($\eta$, $T$) couple, as

$$B = T(\ln \eta - A) \tag{6}$$

where we initially used an estimated value of $A = -11.35$, but then kept $A$ as a fitting parameter to be eventually determined by least-squares optimization. Thus, when fitting Eq. (2) to $B(\mathbf{x})$ data, we obtained values of both $A$ and the first-order coefficients, $B_i$s. For this preliminary fit, the coefficient of determination was $R^2 = 0.9172$.

The fit assigned unrealistically high $B_i$ values for $SO_3$ and some of the 17 minor components for which the mass fraction did not exceed 1 mass% in any glass ($Cs_2O$, $Sb_2O_3$, $SeO_2$, $Tl_2O$, $Tc_2O_7$, $Ag_2O$, $RuO_2$, $Pr_2O_3$, $WO_3$, $As_2O_3$, I, PdO, $Re_2O_7$, $Rh_2O_3$, $Rb_2O$, Br, and $Nb_2O_5$). Because components with $x_i < 0.01$ generally have little impact on viscosity, we removed the mass fractions of these 17 components from the list of viscosity-affecting variables.

To meet the mass-fraction constraint, Eq. (5), for the remaining 39 viscosity-affecting components, we examined two options: either deleting the components with $x_i<0.01$ and renormalizing the mass fractions of the remaining components, or summing the $x_i$s of the removed components into a single component called "*Others*." As expected, the coefficient of determination was marginally lower with the first option ($R^2=0.9172$) than with the second ($R^2=0.9176$). However, the main reason for choosing the second option for subsequent calculations was that having the *Others* component appeared advantageous for the subsequent model development (see Section 6).

Another component with an unrealistically high $B_i$, though with $x_i>0.01$ in several targeted compositions, was $SO_3$. The $B_{SO3}$ value appeared to be the highest of all coefficients and remained extremely high ($B_{SO3}=3.65\times10^4$ K) even after two glasses with >2.0 mass% $SO_3$ were deleted from the database. This impossible value was most likely caused by $SO_3$ segregation and evaporation from the melts as a result of which the targeted content of $SO_3$ was not retained in the glass. The actual $SO_3$ content would thus likely classify $SO_3$ as a minor component. Replacing targeted $SO_3$ fractions with analytical ones did not appear practicable. After some deliberations, we chose to add the $SO_3$ targeted fractions to *Others* while deleting glasses with $x_{SO3}>0.02$. As a result, the number of data decreased to 6755.

### 2.3. Acceptability limit

The $R^2=0.917$ of the preliminary first-order model was rather low, considering the size of the database. Sorting the data according to the value of $\Delta^2=(B_M-B_C)^2$, where the subscripts M and C denote measured and calculated values, respectively, identified data with extremely large deviations between model and measurement. If such outliers were accepted for model generation, they would unduly influence the outcome and increase the model uncertainty for the majority of data.

To define outliers, we established an acceptability limit. Fig. 1 displays the plot of $\Delta^2$ versus $n$, where $n$ is the cumulative number of data sorted by $\Delta^2$ from smallest to largest. To obtain $\Delta^2$, we calculated $B_M$ using Eq. (6) and $B_C$ using Eq. (2) in which $B_i$s and $A$ came from a preliminary first-order model. The $\Delta^2$ values varied by 11 orders of magnitude, from $5.4\times10^{-4}$ K$^2$ to $2.3\times10^7$ K$^2$, i.e., from extremely low values for data for which $B_C$s happened, more or less accidentally, to be nearly identical to $B_M$s, to very large ones for erroneous data not captured by the model. As Fig. 1 shows, the logarithms of $\Delta^2$ increased nearly linearly with $n$ for $n$ between 3000 and 6000 ($\Delta^2$ between $3.2\times10^4$ and $1.3\times10^5$ K$^2$). The obvious candidates for outliers were data with $\Delta^2>3.3\times10^5$ K$^2$. Therefore, we selected $\Delta^2=3.3\times10^5$ K$^2$ as the limit of acceptability (the horizontal line in Fig. 1) and used this limit for all but two models.

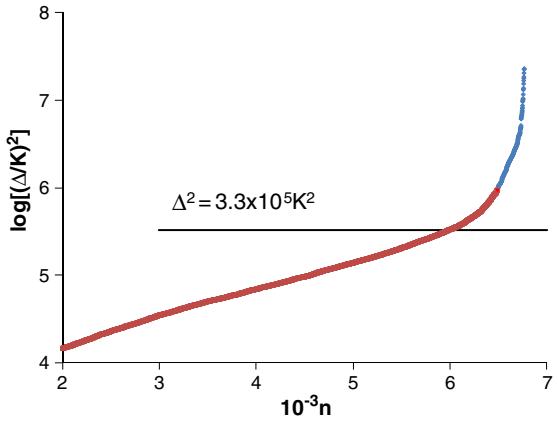


**Fig. 1.** Deviation squared, $\Delta^2=(B_M-B_C)^2$, versus $n$, the number of data sorted by $\Delta^2$.

**Table 1**
Model A component coefficients and the maximum ($x_{im}$) and average ($x_{ia}$) component mass fractions.

| | $10^{-4}$ B$_i$(K) | $x_{im}$ | $x_{ia}$ | | $10^{-4}$B$_i$ (K) | $x_{im}$ | $x_{ia}$ |
|---|---|---|---|---|---|---|---|
| $SiO_2$ | 3.001 | 0.6413 | 0.4606 | $Gd_2O_3$ | 1.485 | 0.0772 | 0.0028 |
| $Na_2O$ | −0.031 | 0.3505 | 0.1294 | $Ce_2O_3$ | 1.824 | 0.0712 | 0.0039 |
| $Fe_2O_3$ | 1.565 | 0.2639 | 0.0527 | F | −0.437 | 0.0600 | 0.0035 |
| $Al_2O_3$ | 3.506 | 0.2663 | 0.0734 | $V_2O_5$ | 1.417 | 0.0599 | 0.0009 |
| SrO | 0.969 | 0.2990 | 0.0057 | $La_2O_3$ | 0.681 | 0.0500 | 0.0023 |
| $K_2O$ | 0.877 | 0.1000 | 0.0142 | BaO | 0.601 | 0.0471 | 0.0018 |
| $B_2O_3$ | 0.352 | 0.2019 | 0.0837 | $Eu_2O_3$ | 1.526 | 0.0436 | 0.0001 |
| CaO | 0.558 | 0.1500 | 0.0303 | $Sm_2O_3$ | 1.607 | 0.0436 | 0.0001 |
| $Bi_2O_3$ | 1.361 | 0.1618 | 0.0015 | CdO | 0.983 | 0.0400 | 0.0018 |
| $ZrO_2$ | 2.712 | 0.1581 | 0.0322 | SnO | 2.034 | 0.0346 | 0.0002 |
| $UO_2$ | 2.096 | 0.1462 | 0.0033 | NiO | 0.397 | 0.0212 | 0.0033 |
| MnO | 0.544 | 0.1360 | 0.0053 | $HfO_2$ | 2.093 | 0.0311 | 0.0000 |
| $P_2O_5$ | 2.631 | 0.1311 | 0.0085 | $Ga_2O_3$ | 2.061 | 0.0302 | 0.0001 |
| $TiO_2$ | 1.318 | 0.0535 | 0.0036 | $Y_2O_3$ | 1.636 | 0.0302 | 0.0001 |
| ZnO | 1.179 | 0.0986 | 0.0095 | CuO | 1.288 | 0.0299 | 0.0004 |
| PbO | 1.036 | 0.0967 | 0.0014 | $Cr_2O_3$ | 1.003 | 0.0297 | 0.0016 |
| MgO | 1.184 | 0.0821 | 0.0094 | CoO | 2.005 | 0.0223 | 0.0001 |
| $Li_2O$ | −3.937 | 0.0899 | 0.0303 | $MoO_3$ | 1.902 | 0.0201 | 0.0013 |
| $Nd_2O_3$ | 2.083 | 0.0838 | 0.0050 | Others | 1.627 | 0.1075 | 0.0131 |
| $ThO_2$ | 1.568 | 0.0781 | 0.0028 | | | | |

For each model, we started computation with the full set of data (original or reduced, see Section 3.2). After the first fitting, we repeatedly removed data exceeding the acceptability limit and refitted the model until the selection of acceptable data stabilized. Model A is a first-order model thus fitted to obtain $B_i$ coefficients for 39 components listed in Table 1. As Table 2 shows, the composition regions of original data and acceptable data are nearly identical. Maximum mass fractions decreased for only 6 components ($SiO_2$, $Fe_2O_3$, $K_2O$, CaO, MgO, and NiO), and minimum mass fractions (0 for all components but $SiO_2$ and $Na_2O$) increased only for $SiO_2$ (from 0.194 to 0.214).

Fig. 2 displays all data points with $\eta<1050$ Pa s on the ($T^{-1}$, log $\eta$) and ($T^{-1}$, $B$) planes. The $T$ spans the interval from 752 to 1806 °C and log($\eta$/Pa s) from −0.85 to 3.02. The $T$ span of Model A acceptable data shrank to the interval from 800 to 1632 °C and the span of log($\eta$/Pa s) ranged from −0.51 to 2.57. Fig. 2 compares acceptable data with all data, and indicates that most of the 856 outliers lie inside the ($T^{-1}$, $B$) region of accepted data.

### 2.4. Composition region and fitting parameters

Model A encompasses all 39 components. Other models use 15 to 24 viscosity-affecting components. Components that are less likely to influence viscosity for most glasses were identified by sorting components according to three criteria, i.e., $B_i-B_a$, $(B_i-B_a)x_{ia}$ and $(B_i-B_a)x_{iM}$, where subscripts $a$ and $M$ stand for average and maximum, respectively. Components $Ce_2O_3$, CoO, $Cr_2O_3$, CuO, $Eu_2O_3$, $Ga_2O_3$, $HfO_2$, $MoO_3$, $Nd_2O_3$, $Sm_2O_3$, SnO, $ThO_2$, $TiO_2$, $UO_2$, $Y_2O_3$ had low values of all the three criteria. After moving these components to *Others*, the composition region shrank to $N=24$ components, including *Others*.

**Table 2**
Comparison of maximum component mass fractions for all data with $\eta>1050$ Pa·s and data with $\Delta^2<3.3\times10^5$ K$^2$.

| Component | All data | Selected data |
|---|---|---|
| $SiO_2$ | 0.716 | 0.641 |
| $Fe_2O_3$ | 0.345 | 0.264 |
| $K_2O$ | 0.210 | 0.100 |
| CaO | 0.182 | 0.150 |
| MgO | 0.096 | 0.082 |
| NiO | 0.030 | 0.021 |

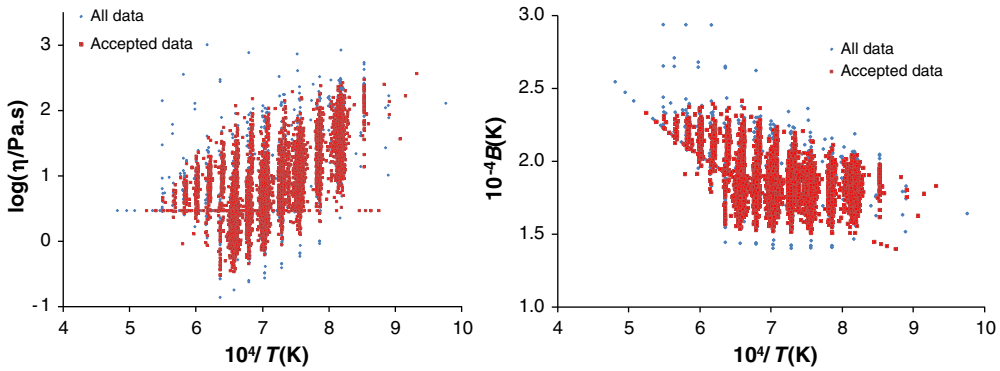


**Fig. 2.** Positions of all data points with $\eta<1050$ Pa·s and data points with $\Delta^2<3.3\times10^5$ K$^2$ (selected data, Model A) on the ($T^1$, log $\eta$) surface (left) and ($T^1$, $B$) surface (right).

Model B is a first-order model fitted to the 24 components. The standard procedure of repeated fitting and $\Delta^2$-sorting until the number of outliers stabilized resulted in 5893 acceptable data points, only marginally less than the number for Model A (5909). Both the $T$ span and log($\eta$/Pa s) interval remained unaffected and the composition region was unchanged except for the maximum mass fraction of $SiO_2$, which decreased to 0.628. The component coefficients are listed in Table 3.

The composition region is a domain in the ($N$-1)-dimensional composition space (by Eq. (5), only $N$-1 composition variables are independent). Here we consider the composition region as an ($N$-1)-dimensional box defined by the ranges of mass fractions of components, i.e., the minimum and maximum values of $x_i$ for each component, even though the measured data are not distributed within the multidimensional box with a representative uniformity. By Eqs. (2) and (4), the number of components limits the number of component coefficients, $B_i$ and $B_{ij}$, of the first- and second-order polynomial terms. The number of nonzero first- and second-order component coefficients, plus 1 for $A$ as an additional fitting parameter, constitutes the number of model parameters, $p$.

## 3. Second-order models

### 3.1. First-order model augmented with second-order terms

For the computation of second-order effects, we selected 8 major components with the highest values of $(B_i-B_a)x_{ia}$ (based on first-order coefficients), namely, $SiO_2$, $Na_2O$, $Li_2O$, $B_2O_3$, $Al_2O_3$, CaO, $ZrO_2$, and $Fe_2O_3$. Thus, the full second-order $B_{ij}$ matrix has $N_2=36$ coefficients. In the baseline Model C, we added these second-order terms to the first-order terms of Model B. Thus, the activation energy for viscosity in second-order models was expressed by the formula

$$B=\sum_{i=1}^{N_1}B_ix_i+\sum_{i=j}^{N_M}\sum_{j=1}^{N_M}B_{ij}x_ix_j \tag{7}$$

**Table 3**
Summary of first-order coefficients, $B_i$, in $10^4$ K. Also included are the number of data selected ($n_s$), the Arrhenius $A$ coefficient, the coefficient of determination ($R^2$), the number of model parameters ($p$), the average activation energy ($B_a$), and the activation energy standard deviation ($S$).

| Model | A[(a)] | B | C | D | E | F | G | H | I | J | K | L | M |
|---|---|---|---|---|---|---|---|---|---|---|---|---|---|
| $n_s$ | 5909 | 5893 | 6239 | 5969 | 5950 | 5867 | 3589 | 1471 | 5839 | 5313 | 6129 | 5764 | 5910 |
| $A$ | −11.23 | −11.19 | −11.42 | −11.44 | −11.43 | −11.37 | −11.29 | −11.24 | −11.49 | −11.06 | −11.37 | −11.39 | −11.429 |
| $R^2$ | 0.9712 | 0.9710 | 0.9804 | 0.9811 | 0.9807 | 0.9795 | 0.9960 | 0.9995 | 0.9803 | 0.9728 | 0.9781 | 0.9784 | 0.9804 |
| $p$ | 40 | 25 | 61 | 61 | 55 | 52 | 52 | 52 | 53 | 31 | 45 | 44 | 38 |
| $10^{-4}B_a$(K) | 1.8711 | 1.8660 | 1.8956 | 1.8981 | 1.8969 | 1.8890 | 1.8810 | 1.8697 | 1.9057 | 1.8469 | 1.7898 | 1.8923 | 1.8966 |
| $10^{-4}S$(K) | 0.1460 | 0.1613 | 0.1523 | 0.1539 | 0.1539 | 0.1537 | 0.1500 | 0.1461 | 0.1534 | 0.1486 | 0.1527 | 0.1527 | 0.1535 |
| $SiO_2$ | 3.00 | 3.00 | 3.09 | 3.05 | 3.05 | 3.15 | 3.15 | 3.15 | | | | | 4.03 |
| $Na_2O$ | −0.03 | −0.04 | −0.34 | −0.26 | −0.20 | −0.22 | −0.22 | −0.22 | | | | | 1.05 |
| $B_2O_3$ | 0.35 | 0.32 | 0.29 | 0.40 | 0.45 | 0.37 | 0.37 | 0.37 | | | | | 1.24 |
| $Al_2O_3$ | 3.51 | 3.50 | 3.48 | 3.43 | 3.36 | 3.27 | 3.27 | 3.27 | | | | | 3.87 |
| $Fe_2O_3$ | 1.57 | 1.55 | 0.81 | 0.78 | 0.80 | 0.53 | 0.53 | 0.53 | | | | | 1.62 |
| $ZrO_2$ | 2.71 | 2.71 | 1.86 | 1.77 | 1.68 | 1.54 | 1.54 | 1.54 | | | | | 2.00 |
| $Li_2O$ | −3.94 | −3.91 | −4.52 | −4.43 | −4.37 | −4.38 | −4.38 | −4.38 | | | | | −3.88 |
| CaO | 0.56 | 0.53 | 0.08 | 0.07 | −0.01 | 0.17 | 0.17 | 0.17 | | | | | 0.92 |
| SrO | 0.97 | 1.01 | 1.04 | 1.03 | 1.02 | 0.74 | 0.74 | 0.74 | 2.48 | 2.33 | 2.32 | 2.04 | 0.37 |
| $K_2O$ | 0.88 | 0.80 | 0.99 | 1.02 | 1.00 | 1.03 | 1.03 | 1.03 | 2.54 | 2.49 | 2.53 | 2.51 | 0.26 |
| $Bi_2O_3$ | 1.36 | 1.43 | 1.46 | 1.57 | | | | | 2.85 | | | | 1.07 |
| MnO | 0.54 | 0.46 | 0.77 | 0.77 | 0.79 | | | | 2.17 | 1.75 | 2.15 | | 0.07 |
| $P_2O_5$ | 2.63 | 2.64 | 2.67 | 2.69 | 2.70 | 2.64 | 2.64 | 2.64 | 4.26 | 4.13 | 4.20 | 4.23 | 1.99 |
| ZnO | 1.18 | 1.03 | 1.59 | 1.54 | 1.66 | 1.59 | 1.59 | 1.59 | 3.10 | 3.65 | 3.26 | 3.24 | 0.78 |
| PbO | 1.04 | 0.98 | 1.29 | 1.13 | | | | | 0.61 | | | | 0.14 |
| MgO | 1.18 | 1.15 | 1.23 | 1.28 | 1.28 | 1.37 | 1.37 | 1.37 | 2.78 | 2.91 | 2.76 | 2.82 | 0.54 |
| $Gd_2O_3$ | 1.49 | 1.27 | 1.64 | 1.60 | | | | | 2.94 | 3.13 | | | 1.21 |
| F | −0.44 | −0.47 | 0.21 | 0.24 | 0.08 | −0.01 | −0.01 | −0.01 | 1.63 | 2.34 | 1.72 | 1.93 | −0.47 |
| $V_2O_5$ | 1.42 | 1.40 | 1.85 | 1.78 | | | | | 1.28 | | | | |
| $La_2O_3$ | 0.68 | 0.66 | 1.19 | 1.22 | | | | | 2.70 | 3.03 | | | 0.39 |
| BaO | 0.60 | 0.66 | 1.22 | 1.30 | | | | | 2.76 | 2.66 | | | 0.57 |
| CdO | 0.98 | 0.74 | 1.18 | 1.15 | 0.70 | | | | 2.06 | 2.43 | | | 0.26 |
| NiO | 0.40 | 0.79 | 1.17 | 1.14 | 1.19 | | | | 3.64 | 3.01 | | | 0.60 |
| Others | 1.63 | 1.77 | 1.84 | 1.87 | 1.77 | 1.65 | 1.65 | 1.65 | 3.27 | 2.97 | 3.02 | 3.04 | 1.18 |

(a) See Table 2 for additional coefficients.

where $N_M$ is the number of major components, $N_1 = N_{M1} + N_m$ is the number of the nonzero first-order coefficients, $N_{M1}$ is the number of first-order terms for major components, and $N_m$ is the number of viscosity-affecting minor components, including *Others*. Since $N_2 = (1/2)N(N+1)$, while some second-order terms can be zero (as in Model J described below), $N_2$ includes both nonzero terms and terms with $B_{ij} = 0$. The second-order coefficients are listed in Table 4.

In Model C, we kept all the first-order terms of Model B, including those of the 8 major components (see Table 3). These terms would be, by Eq. (3), redundant in the full second-order model. However, because 16 components (SrO, $K_2O$, $Bi_2O_3$, MnO, $P_2O_5$, ZnO, PbO, MgO, $Gd_2O_3$, F, $V_2O_5$, $La_2O_3$, BaO, CdO, NiO, and *Others*) are represented solely by first-order terms, we reasoned that the lack of missing interactions of these components with the main components can be mitigated by retaining the first-order terms for the main components.

Clearly, if an $i$th component does not interact with any other component, then $\bar{B}_{ij} = B_i$ for $j = 1, 2, \ldots, N$ and, by Eq. (5), Eq. (3) reduces to identity. However, if only some components are non-interacting ($N > N_m > 0$), then, for the interacting components, the number of terms in Eq. (3) does not decrease to only those of the double sum in Eq. (7) even in the simple case of a symmetrical $\bar{B}_{ij}$ matrix. Thus, if ($j = 1,2,\ldots,N_M$) components are interacting and ($j = N_M + 1$, $N_M + 2,\ldots N$) components are non-interacting, then, in the case of a symmetrical $\bar{B}_{ij}$ matrix, i.e., $\bar{B}_{ij} = \bar{B}_{ji}$, Eq. (3) becomes $B_i = \sum_{j=1}^{N_M} \bar{B}_{ij} x_j + \bar{B}_i \sum_{j=N_M+1}^{N} x_j$. Hence, the non-interacting components influence the interacting ones by their very presence in the mixture. Obviously, introducing this expression into Eq. (2) will not lead to Eq. (7). Consequently, the empirical coefficients, $B_{ij}$, of Eq. (7) are not equivalent to the averaged partial specific activation energies, $\bar{B}_{ij}$, defined by Eq. (3). A better understanding of Eq. (7) is viewing it as a first-order model augmented with second-order terms.

### 3.2. Description of models

The baseline Model C has 61 coefficients. After fitting it to data, the number of outliers stabilized at $\Delta^2 > 3.3 \times 10^5$ K$^2$ with 6239 data points accepted. Thus, Model C fitted 346 more data than the first-order Model B and 330 more than Model A, indicating that some first-order model outliers (~5% of the database) were excluded because first-order models do not take into account component interactions. The $x_i$ ranges of Model C remained the same as for the first-order models, indicating that first-order-model outliers accepted as valid by the second-order model lay within the inner composition region.

Ten versions of the second-order model were subsequently developed. These models are versions of Model C truncated by various means—see Tables 3 and 4. Only one model (Model K) was fitted to the original base of 6755 data. The other nine models were fitted to a reduced base. This was done in two steps. First, we removed 516 outliers of Model C from the original database. Then, we removed glasses with excessive content of otherwise minor components, because large fractions of these components can bring about nonlinear effects on viscosity while typical HLW glasses do not contain excessive fractions of these components. As seen in Table 5, the maximum fraction ($x_{iM}$) of $Bi_2O_3$, $V_2O_5$, PbO, SrO, $Gd_2O_3$, BaO, MnO, and $La_2O_3$ exceeded the average fraction ($x_{ia}$) by more than 20 times. Thus, we proceeded by removing compositions with $x_{iM}/x_{ia} > 20$, one component

**Table 4**
Summary of second-order coefficients, $B_{ij}$, in $10^4$ K.

| Model | C | D | E | F | G | H | I | J | K | L | M |
|---|---|---|---|---|---|---|---|---|---|---|---|
| $SiO_2 \times SiO_2$ | 0.33 | 0.40 | 0.43 | 0.27 | 0.58 | 0.69 | 3.89 | 4.13 | 3.90 | 3.85 | −0.59 |
| $SiO_2 \times Na_2O$ | −1.26 | −1.43 | −1.58 | −1.66 | −1.86 | −1.54 | −0.12 | −2.37 | −0.25 | −0.02 | −3.63 |
| $SiO_2 \times B_2O_3$ | −0.97 | −1.10 | −1.29 | −1.28 | −1.23 | −1.22 | 1.95 | | 1.58 | 1.60 | −2.75 |
| $SiO_2 \times Al_2O_3$ | 0.51 | 0.66 | 0.74 | 0.88 | 0.90 | 0.92 | 7.68 | 9.47 | 7.87 | 7.70 | −1.06 |
| $SiO_2 \times Fe_2O_3$ | 0.45 | 0.56 | 0.56 | 0.62 | 1.31 | 1.42 | 4.80 | 5.15 | 4.94 | 4.80 | −1.44 |
| $SiO_2 \times ZrO_2$ | 1.62 | 1.79 | 1.97 | 2.29 | 3.15 | 3.08 | 7.25 | 9.79 | 7.73 | 7.59 | |
| $SiO_2 \times Li_2O$ | −4.59 | −4.78 | −4.95 | −5.11 | −5.74 | −5.81 | −8.98 | −10.99 | −9.17 | −8.65 | −7.07 |
| $SiO_2 \times CaO$ | −0.49 | −0.44 | −0.38 | −0.56 | −1.17 | −1.40 | 1.72 | | 1.46 | 1.73 | −2.00 |
| $Na_2O \times Na_2O$ | 1.87 | 1.92 | 1.95 | 1.99 | 1.93 | 1.89 | 2.76 | 4.42 | 2.93 | 2.71 | |
| $Na_2O \times B_2O_3$ | −1.90 | −2.02 | −2.03 | −1.95 | −2.42 | −2.70 | −0.84 | 5.10 | −0.88 | −0.93 | −4.19 |
| $Na_2O \times Al_2O_3$ | 0.29 | 0.19 | 0.10 | 0.14 | 0.21 | 0.54 | 2.74 | | 2.17 | 2.59 | |
| $Na_2O \times Fe_2O_3$ | 1.81 | 1.80 | 1.77 | 1.96 | 2.28 | 2.33 | 2.80 | | 2.53 | 2.23 | |
| $Na_2O \times ZrO_2$ | 1.86 | 1.95 | 1.95 | 1.96 | 2.10 | 2.15 | 3.65 | | 2.52 | 2.79 | |
| $Na_2O \times Li_2O$ | 12.05 | 12.12 | 12.10 | 11.97 | 11.81 | 11.73 | 11.75 | 18.86 | 13.21 | 11.56 | 9.58 |
| $Na_2O \times CaO$ | 2.96 | 2.99 | 3.14 | 2.96 | 2.81 | 2.55 | 4.36 | 12.93 | 5.140 | 4.57 | |
| $B_2O_3 \times B_2O_3$ | 4.35 | 4.17 | 4.28 | 4.33 | 4.00 | 3.83 | 4.15 | 6.93 | 4.76 | 4.97 | 2.87 |
| $B_2O_3 \times Al_2O_3$ | −1.13 | −1.28 | −1.31 | −1.27 | −2.08 | −2.26 | 2.41 | | 2.55 | 2.45 | −2.61 |
| $B_2O_3 \times Fe_2O_3$ | 1.86 | 1.87 | 1.83 | 2.20 | 3.02 | 3.13 | 2.83 | | 2.74 | 2.77 | |
| $B_2O_3 \times ZrO_2$ | 0.62 | 0.67 | 0.68 | 0.53 | 0.50 | 0.65 | 3.10 | | 2.40 | 2.23 | |
| $B_2O_3 \times Li_2O$ | 1.16 | 1.29 | 1.43 | 1.45 | 2.18 | 2.32 | −0.96 | | −0.40 | −1.29 | |
| $B_2O_3 \times CaO$ | 1.02 | 1.06 | 1.04 | 0.93 | 0.68 | 0.71 | 2.26 | | 2.13 | 2.30 | |
| $Al_2O_3 \times Al_2O_3$ | 0.81 | 0.89 | 1.10 | 0.98 | 1.02 | 1.13 | 4.66 | 3.00 | 4.36 | 4.46 | |
| $Al_2O_3 \times Fe_2O_3$ | 1.69 | 1.73 | 1.67 | 1.91 | 1.97 | 1.93 | 6.53 | 7.54 | 5.80 | 6.31 | |
| $Al_2O_3 \times ZrO_2$ | 0.46 | 0.44 | 0.45 | 0.46 | 0.39 | 0.42 | 5.02 | | 5.83 | 6.38 | |
| $Al_2O_3 \times Li_2O$ | −8.76 | −8.83 | −8.87 | −8.81 | −9.12 | −9.16 | −10.94 | −9.44 | −11.40 | −11.73 | −7.78 |
| $Al_2O_3 \times CaO$ | −0.65 | −0.84 | −0.91 | −1.12 | −1.45 | −1.56 | 1.24 | | 0.71 | 0.85 | −2.24 |
| $Fe_2O_3 \times Fe_2O_3$ | 1.17 | 1.12 | 1.02 | 1.43 | 1.25 | 0.98 | 0.31 | 0.94 | 0.60 | 0.84 | |
| $Fe_2O_3 \times ZrO_2$ | 0.27 | 0.02 | 0.02 | −0.09 | 0.16 | 0.34 | 0.35 | | 1.58 | 1.55 | |
| $Fe_2O_3 \times Li_2O$ | −1.62 | −1.52 | −1.47 | −1.49 | −0.91 | −0.82 | −5.25 | | −6.93 | −7.44 | |
| $Fe_2O_3 \times CaO$ | 1.23 | 1.27 | 1.35 | 1.60 | 1.77 | 1.93 | 2.07 | | 1.59 | 2.03 | |
| $ZrO_2 \times ZrO_2$ | −0.92 | −0.91 | −1.00 | −1.17 | −1.16 | −1.21 | −0.50 | | −0.16 | −0.20 | |
| $ZrO_2 \times Li_2O$ | −2.63 | −2.76 | −2.82 | −2.79 | −3.16 | −3.20 | −6.39 | −13.23 | −8.98 | −8.80 | |
| $ZrO_2 \times CaO$ | 1.03 | 1.09 | 0.98 | 0.85 | 0.48 | 0.39 | 2.34 | | 0.58 | 0.94 | |
| $Li_2O \times Li_2O$ | 27.68 | 27.70 | 27.79 | 27.82 | 28.26 | 28.36 | 25.49 | 23.26 | 24.77 | 26.46 | 30.30 |
| $Li_2O \times CaO$ | 5.81 | 5.89 | 5.90 | 6.08 | 6.19 | 6.15 | 5.45 | | 7.12 | 5.82 | |
| $CaO \times CaO$ | 0.38 | 0.47 | 0.61 | 0.38 | 1.14 | 1.42 | 1.67 | | 2.02 | 1.68 | |

**Table 5**
Maximum and average mass fractions of minor components.

| | Original database | | | Reduced database | |
|---|---|---|---|---|---|
| | $x_{iM}$ | $x_{ia}$ | $x_{iM}/x_{ia}$ | $x_{iM}$ | $x_{ia}$ |
| $Bi_2O_3$ | 0.1618 | 0.0015 | 108.6 | 0.0240 | 0.0009 |
| $V_2O_5$ | 0.0599 | 0.0008 | 72.3 | 0.0036 | 0.00003 |
| PbO | 0.0967 | 0.0015 | 65.4 | 0.0106 | 0.0010 |
| SrO | 0.2990 | 0.0061 | 49.3 | 0.1010 | 0.0056 |
| $Gd_2O_3$ | 0.0772 | 0.0024 | 31.7 | 0.0476 | 0.0024 |
| BaO | 0.0471 | 0.0019 | 25.0 | 0.0391 | 0.0017 |
| MnO | 0.1360 | 0.0056 | 24.4 | 0.0702 | 0.0051 |
| $La_2O_3$ | 0.0500 | 0.0025 | 20.4 | 0.0500 | 0.0026 |
| CdO | 0.0400 | 0.0020 | 20.0 | 0.0400 | 0.0020 |
| F | 0.0600 | 0.0037 | 16.4 | 0.0600 | 0.0035 |
| $P_2O_5$ | 0.1311 | 0.0086 | 15.2 | 0.1311 | 0.0087 |
| $K_2O$ | 0.2099 | 0.0145 | 14.5 | 0.1000 | 0.0142 |
| ZnO | 0.0986 | 0.0092 | 10.7 | 0.0821 | 0.0091 |
| MgO | 0.0963 | 0.0096 | 10.0 | 0.0986 | 0.0092 |

at a time, until the $x_{iM}$s decreased to values listed in Table 5. The maximum fractions of all other components except for $K_2O$ and ZnO remained unaffected. The final number of data was 5969. Fig. 3 compares the reduced database with the original one. The reduced database made it possible to further decrease the number of viscosity-affecting components in some models.

To decrease the number of model parameters, we added less-influential components to *Others* in Models E, F, G, H, K, and L and removed the first-order terms of major components in Models I, J, K, and L. Also, we removed selected second-order terms in Models J and M. Finally, we fitted Models G and H to severely restricted ranges of data by reducing the acceptability limit. The 10 model variations are briefly characterized below.

*Model D*. This model is a version of Model C with respect to the kind and number of component coefficients except that it was fitted to the reduced database.
*Model E*. Here we added to *Others* minor components $V_2O_5$, $Bi_2O_3$, PbO, $Gd_2O_3$, BaO, and $La_2O_3$, for which the value of $x_a|B_i - B_a|/B_a$ was smaller than that for *Others* (8.0).
*Model F*. In this model, we added to *Others* all minor components except SrO, $K_2O$, $P_2O_5$, ZnO, MgO, and F.
*Model G*. With the same set of data and coefficients as in Model F, we restricted the model to data using a lower acceptability limit of $\Delta^2 < 3.3\times10^4$ K$^2$.

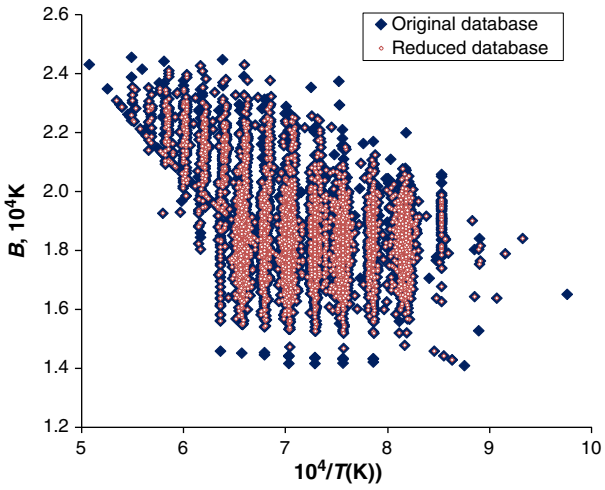


**Fig. 3.** Positions of all data points with $\eta < 1050$ Pa·s and $\Delta^2 < 3.3\times10^5$ K$^2$ of original database and reduced database on the ($T^1$, $B$) surface.

*Model H*. In this model, we further reduced the acceptability limit to $\Delta^2 < 3.3\times10^3$ K$^2$.
*Model I*. To examine the influence of the first-order terms of the main components in a second-order model, we removed these terms from Model D while keeping the list of minor components unchanged.
*Model J*. In this version of Model I, we removed less-influential second-order terms, those with $x_{iM}x_{jM}(B_{ij} - B_a)/B_a < 0.399$. Also, we added to *Others* three minor components, $Bi_2O_3$, PbO, and $V_2O_5$.
*Model* K. This is the only second-order model other than Model C fitted to the original database. In addition to removing first-order terms of the main components, we also removed several minor components and added them to *Others*.
*Model L*. Here we removed from Model F the first-order coefficients of the major components.
*Model M*. This model is based on Model D except that, like Model J, it does not have $B_{ij}$ coefficients for less-influential terms (those with $x_{iM}x_{jM}(B_{ij} - B_a)/B_a < 0.07$) and $V_2O_5$ was added to *Others*.

The component coefficients for all models are listed in Tables 3 and 4. Table 3 also lists values of $A$, $R^2$, $p$, and other parameters.

## 4. Component effects

### 4.1. Component replacement and component addition

To determine the $k$th component effect, we first single this component out, rewriting Eq. (7) as

$$B = B_k x_k + \sum_{i\neq k} B_i x_i + B_{kk}x_k^2 + x_k \sum_{i\neq k} B_{ik}x_i + \sum_{i\neq k}^{N_M}\sum_{j\neq k}^{N_M} B_{ij}x_i x_j \quad (8)$$

where the first-order terms $B_i x_i$ are summed from $i = 1$ to $i = N_1$ ($i \neq k$) and the terms $B_{ik}x_i$ are summed from $i = 1$ to $i = N_M$ ($i \neq k$). Second, we obtain the derivative with respect to $x_k$ as follows

$$\frac{\partial B}{\partial x_k} = B_k + \sum_{i\neq k} B_i \frac{\partial x_i}{\partial x_k} + 2B_{kk}x_k + \sum_{i\neq k} B_{ik}x_i + x_k \sum_{i\neq k} B_{ik}\frac{\partial x_i}{\partial x_k} + \sum_{i\neq k}^{N_M}\sum_{j\neq k}^{N_M} B_{ij}\left(\frac{\partial x_i}{\partial x_k}x_j + \frac{\partial x_j}{\partial x_k}x_i\right) \quad (9)$$

As Eq. (9) indicates, a component affects $B$ depending to according to which other components it replaces, i.e., $\partial B/\partial x_k$ is a function $\partial x_i/\partial x_k$ ($i \neq k$). Here we will consider two simple cases.

1) *Component replacement*. In the simplest case, an increase in $x_i$ is compensated by a decrease of another component, for example, increasing the $K_2O$ content at the expense of $Na_2O$ while the contents of all remaining $N$-2 components remain unchanged.
2) *Component addition*. Alternatively, a component is added to the mixture, while fractions of all other components are decreased in equal proportions.

Note that composition changes that increase $B$ also increase $\eta$, provided that $T$ = constant. This follows from Eqs. (1) and (2). Combining these equations and using Eq. (5), we can write $\ln\eta = \sum_{i=1}^{N} f_i x_i$, where $f_i = A + B_i/T$. Thus, at any temperature at which $\eta < 10^3$ Pa s, the $i^{th}$ component for $\ln(\eta)$, $f_i$, is proportional to the corresponding $i^{th}$ component for $B$.

The following two sections deal with the two cases, component replacement and component addition.

### 4.2. Component replacement: Changing $x_k$ for $x_j$

In the case of changing $x_k$ for $x_j$, we have $dx_j/dx_k = -1$ and $dx_i/dx_k = 0$ for all $i \neq j$ and $i \neq k$. Thus, Eq. (9) yields

$$\frac{\partial B}{\partial x_k} = B_k - B_j + B_{kk}x_k - B_{jj}x_j + \sum_{i=1}^{N_M} B_{ik}x_i - \sum_{i=1}^{N_M} B_{ij}x_i \tag{10}$$

The second derivative is

$$\frac{\partial^2 B}{\partial x_k^2} = 2\left(B_{kk} - B_{kj} + B_{jj}\right) \tag{11}$$

For the first-order model, Eq. (10) reduces to a simple relation, $\partial B/\partial x_k = B_k - B_j$, whereas for the second-order model, the component effect consists of multiple terms even in the simple case of exchanging one component with another. This is because each major component affects each other.

### 4.3. Component addition: adding $x_k$ to mixture

In the case of the $k$th component added to the mixture, concentrations of all other components remain in the same proportions as in the reference mixture. Hence,

$$\frac{\partial x_i}{\partial x_k} = -\frac{x_{iR}}{1 - x_{kR}} \tag{12}$$

where the subscript R denotes the reference mixture. Then Eq. (9) becomes

$$\frac{\partial B}{\partial x_k} = B_k + 2B_{kk}x_k + \sum_{i\neq k} B_{ik}x_i - \frac{\sum_{i\neq k} B_i x_{iR} + x_k \sum_{i\neq k} B_{ik}x_{iR} + \sum_{i\neq k}^{N_M}\sum_{j\neq k}^{N_M} B_{ij}\left(x_{iR}x_j + x_{jR}x_i\right)}{1 - x_{kR}} \tag{13}$$

Combining Eqs. (8) and (13), we obtain for the component effect at the reference mixture the expression

$$\left.\frac{\partial B}{\partial x_k}\right|_R = \frac{B_k - B_R + B_{kk}x_{kR} - \sum_{i\neq k}^{N_M}\sum_{j\neq k}^{N_M} B_{ij}x_{iR}x_{jR}}{1 - x_{kR}} + \sum_{i=1}^{N_M} B_{ki}x_{iR} \tag{14}$$

This rather complicated expression simplifies for first-order models to $\beta_i = \partial B/\partial x_i = (B_i - B_a)/(1 - x_{ia})$, where the centroid or average composition was chosen as reference ($B_a$ and $x_{ia}$ are averages of $B$s and $x_i$s for all compositions within the model composition region— the formulas are given in Sections 4.6 and 6). Table 6 lists $\beta_i$ values for Models A and B.

### 4.4. First-order mixture component classification

Denoting $B_m$ and $B_M$ as the smallest and the largest experimental values of $B$ in the composition region, it follows that components with $B_i < B_m = 1.4\times10^4$ K decrease and components with $B_i > B_M = 2.4\times10^4$ K increase the value of $B$ when added to any glass with a composition within the composition region.

The $\beta_i$ values of first-order models allow classification of glass components into the following groups:

- Components that strongly decrease $B$ are $Li_2O$ ($\beta_{Li2O} = -6.0\times10^4$ K), F, $Na_2O$, and $B_2O_3$.
- Components that moderately decrease $B$ ($\beta_i \leq -1.2\times10^4$ K) are NiO, CaO, MnO, BaO, and $La_2O_3$.

**Table 6**
Summary of component effects expressed as $(B_i\text{-}B_a)/(1\text{-}x_a)$ in $10^4$ K.

| Model | A | B | Model | A | B |
|---|---|---|---|---|---|
| $SiO_2$ | 2.094 | 2.101 | $Gd_2O_3$ | −0.387 | −0.596 |
| $Na_2O$ | −2.185 | −2.185 | $Ce_2O_3$ | −0.047 | |
| $Fe_2O_3$ | −0.323 | −0.330 | F | −2.316 | −2.343 |
| $Al_2O_3$ | 1.764 | 1.764 | $V_2O_5$ | −0.454 | −0.470 |
| SrO | −0.907 | −0.863 | $La_2O_3$ | −1.193 | −1.213 |
| $K_2O$ | −1.008 | −1.079 | BaO | −1.272 | −1.206 |
| $B_2O_3$ | −1.658 | −1.688 | $Eu_2O_3$ | −0.345 | |
| CaO | −1.354 | −1.374 | $Sm_2O_3$ | −0.264 | |
| $Bi_2O_3$ | −0.511 | −0.442 | CdO | −0.890 | −1.128 |
| $ZrO_2$ | 0.869 | 0.869 | SnO | 0.163 | |
| $UO_2$ | 0.226 | | NiO | −1.479 | −1.084 |
| MnO | −1.334 | −1.415 | $HfO_2$ | 0.222 | |
| $P_2O_5$ | 0.766 | 0.785 | $Ga_2O_3$ | 0.190 | |
| $TiO_2$ | −0.555 | | $Y_2O_3$ | −0.235 | |
| ZnO | −0.699 | −0.840 | CuO | −0.583 | |
| PbO | −0.836 | −0.889 | $Cr_2O_3$ | −0.870 | |
| MgO | −0.694 | −0.722 | CoO | 0.134 | |
| $Li_2O$ | −5.990 | −5.955 | $MoO_3$ | 0.031 | |
| $Nd_2O_3$ | 0.213 | | Others | −0.247 | −0.098 |
| $ThO_2$ | −0.304 | | | | |

- Components that slightly decrease $B$ ($\beta_i \leq -0.84\times10^4$ K) are $K_2O$, SrO, CdO, $Cr_2O_3$, and PbO.
- Components that marginally decrease $B$ ($\beta_i \leq -0.35\times10^4$ K) are ZnO, MgO, CuO, $TiO_2$, $Bi_2O_3$, $V_2O_5$, and $Gd_2O_3$.
- Components that strongly increase $B$ are $SiO_2$ ($\beta_{SiO2} = 2.1\times10^4$ K), $Al_2O_3$, $ZrO_2$, and $P_2O_5$.
- All other components listed ($Eu_2O_3$, $Fe_2O_3$, $ThO_2$, $Sm_2O_3$, $Y_2O_3$, $Ce_2O_3$, $MoO_3$, CoO, SnO, $Ga_2O_3$, $Nd_2O_3$, $HfO_2$, $UO_2$, and those in *Others*) have a miniscule impact and may increase or decrease $B$ depending on the composition to which they are added ($-0.35\times10^4 K < \beta_i < 0.25\times10^4$ K).

Note that out of all minor components (by concentration), only F and $P_2O_5$ have a strong effect on viscosity.

### 4.5. Model-to-model variations of component coefficients

Numerous observations can be made based on the component coefficients and component effects as listed below.

- The influence of *Others* is lower in Model B ($\beta_{Others} = -0.10\times10^4$ K) than in Model A, ($\beta_{Others} = -0.25\times10^4$ K), even though *Others* in Model B contain 15 more components than *Others* in Model A. The cause of this is a mutual compensation of the effects of components within *Others*.
- Based on the component effects, alkali oxides affect $B$ in the order $Li_2O < Na_2O < K_2O$. No such correlation exists between $B_i$ and the atomic mass in other groups of oxides, such as MgO–CaO–SrO–BaO, or $TiO_2$–$ZrO_2$–$HfO_2$–$ThO_2$.
- Note that $Li_2O$ exhibits a stronger nonlinear behavior than other components. It interacts mainly with $SiO_2$, $Al_2O_3$, and $Na_2O$ (see the large $B_{ij}$ values with $i \equiv SiO_2$, $Al_2O_3$, $Na_2O$, and $Li_2O$ and $j \equiv Li_2O$).
- As the comparison between the Model C and D coefficients indicates (see Table 3) and as Fig. 4 illustrates, removing 270 data with extreme compositions of otherwise minor components (called semiminor in Fig. 4 legend) had little impact on the model while the $R^2$ marginally increased.
- When only influential second-order components were selected in Models J and M, some second-order coefficients changed significantly, as can be seen by comparing the $B_{ij}$ values of Models I and J and Models M and D (see Tables 3 and 4).
- Reducing the number of linear terms had a noticeable effect on some first-order coefficients—compare $B_F$ (F stands for fluorine) and $B_{CaO}$ of Models E and F versus Model D. However, no such striking difference appears between Models K and L versus Model I.

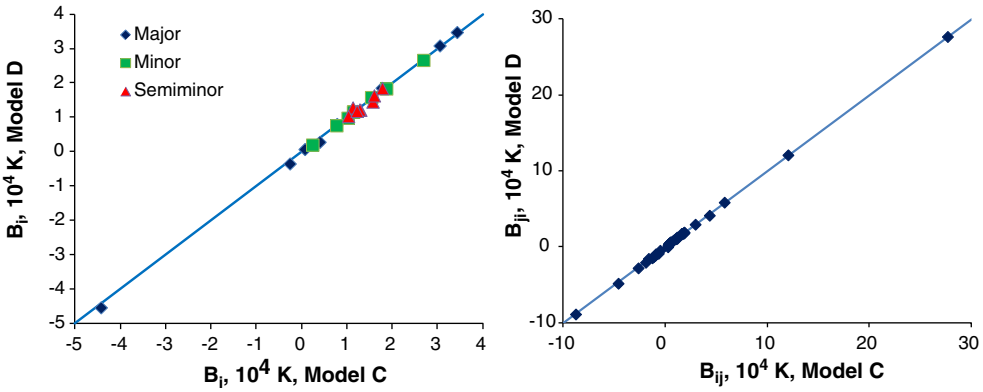


**Fig. 4.** Component coefficients based on reduced (Model D) versus original (Model C) database.

- Removing the first-order terms of major coefficients that are represented by the full set of second-order terms affects both $B_i$ and $B_{ij}$ coefficients.

Regarding the model-to-model differences of the coefficients, one can think about two contributing factors:

1) Insufficient coverage of certain components by data can make their coefficients sensitive to experimental errors that mimic the effect of composition. This can also be an unintentional consequence of changes caused by removing outliers.
2) Coefficients in a mixed first and second-order model are not uniquely determined. Let Q be an arbitrary number and

$$B = \sum_{i=1}^{N} B_i x_i + \sum_{i=1}^{N}\sum_{j=1}^{N} \bar{B}_{ij} x_i x_j \tag{7a}$$

Eq. (7a) yields an identical $B$ value if $B_i$ is replaced with $B_i + Q$ and $\bar{B}_{ij}$ with $\bar{B}_{ij} - Q$. This follows from the identity $\sum_{i=1}^{N}\sum_{j=1}^{N} x_i x_j = 1$. The lack of uniqueness of $B_i$ and $\bar{B}_{ij}$ values in Eq. (7a) can lead to substantial differences in coefficient values without affecting the model outcome.

Both first- and second-order coefficients significantly differ between Models D and M. As Fig. 5 shows, first-order coefficients of major components of Model M are all larger than the corresponding coefficients of Model D, whereas the values of all but two second-order coefficients are lower. On the other hand, the first-order coefficients of minor components of Model M are all larger than the corresponding coefficients of Model D. The differences between the corresponding coefficients are similar, though not exactly equal, but an exact equality is not expected because the coefficients do not make a complete set as in Eq. (7a) and Model M has a lower number of parameters (38) than Model D (61). Yet the outcome of these two models is close (see Fig. 5c), only the outliers are estimated somewhat differently.

### 4.6. Spider plots

Finally, Fig. 6 displays the effects of several glass components in terms of $B$ versus the mass fractions of various components added to the average composition. The $i$th component mass fraction in the average glass is $x_{ia} = n_s^{-1}\sum x_i$, where the summation is over all glasses on which the model is based (e.g., $n_s = 5867$ for Model F). With the $k$th component added in the amount $\Delta x_k = x_k - x_{ka}$, the $i$th component mass fraction in the new glass is $x_i = x_{ia}(1 - x_k)/(1 - x_{ka})$. Fig. 6 displays the $B$ values as a function of $\Delta x_k$. The slopes of the lines at $\Delta x_k = 0$ (the average glass) are given by Eq. (14). The diagram in Fig. 6, also called a spider plot, is based on Model F coefficients. Note that the effects of $B_2O_3$, CaO, and SrO are similar.

### 4.7. Glass length

According to the traditional glassmakers' parlance, glass is called "long" if its viscosity decreases slowly with time during which a glass blob is workable on the glassblower's pipe. Thus, the less the viscosity increases with decreasing temperature as the glass blob cools, the "longer" is the glass. Hence, we can define the glass length as $\lambda = \partial \ln(\eta)/\partial(1/T)$. Extending this term from the glass-forming temperature interval to the glass-making one, or disregarding the change of $B$ with $T$ when $\eta > 10^3$ Pa s, it follows from Eq. (1) that $\lambda = B(\mathbf{x})$.

To demonstrate how the glass length depends on glass composition, we need to express the derivative of $\lambda$ with respect to the $i$th component fraction. Replacing $n$th component with $i$th components and using the first-order model, we obtain

$$\frac{\partial \lambda}{\partial x_i} = B_i - B_n \tag{15}$$

Thus, glass length will increase if $B_i > B_n$. According to Table 3 data, $Al_2O_3$ makes the glass longer and $LiO_2$ makes it shorter when replacing any of the remaining 38 components of Model A.

## 5. Number of parameters and number of data accepted

The number of model parameters, $p = N_1 + N_{02} + 1$, where $N_{02}$ is the number of nonzero second-order coefficients, is listed in Table 3 together with the number of data accepted, $n_s$ (the number of data minus the number of outliers). For models with the reduced database (Models D, E, F, I, J, and L), $n_s$ increases as $p$ increases. The lower line in Fig. 7 was fitted with the equation

$$n_s = n_R\left[1 - A_p \exp(-p/p_1)\right] \tag{16}$$

where $n_R = 5969$ is the number of all data in the reduced database, and $A_p$ and $p_1$ are coefficients whose values are $A_p = 1.863$ and $p_1 = 10.85$. The number of parameters at which no data would be accepted, provided that Eq. (16) can be extrapolated, is $p_0 = p_1 \ln(A_p) = 6.75$. Models fitted to the original database (A, C, and K) and Model M fall on a similar line (using the same vales of $A_p$ and $p_1$ while setting $n_R = 6266$), but Model B covers nearly as many data as Model A.

Regarding individual models, one can make the following observations.

Two second-order models, C and K, fit the highest number of data with $\eta < 1050$ Pa s (92% and 91%, respectively), even though Model K

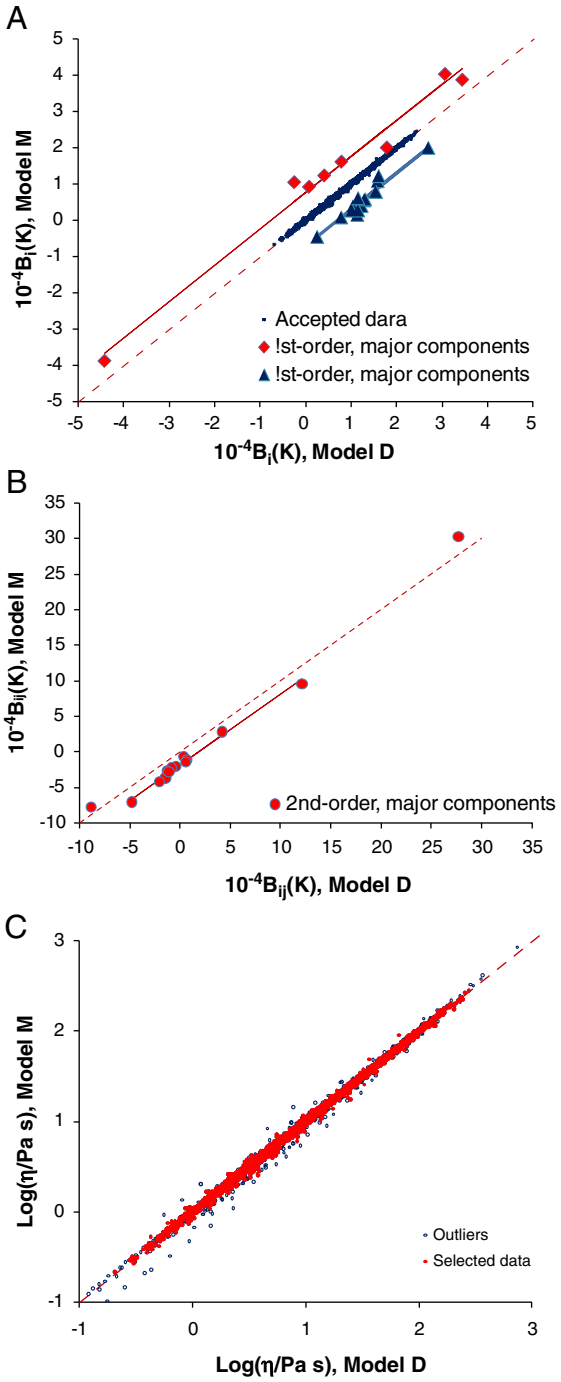


**Fig. 5.** Model M versus Model D comparison of first-order coefficients (A), second-order coefficients (B) and estimated viscosities (C).

has no first-order coefficients for major components and has only 45 parameters (compared to 61 of Model C). Similarly, both first-order models, A and B, cover 87% of all data in spite of the difference in the number of components evaluated (39 versus 24).

Model D, with an equal number of parameters to Model C (61), but fitted to a truncated composition region (the reduced database, Table 5), covers a significantly smaller number of data (88% of all data), though only 1% more than Model B with an equal number of components, but only 25 parameters, or Model M with 38 parameters. Similarly, Model L with a $p$ value close to that of Model K (44 and 45, respectively), but fitted to the reduced database, covers a substantially smaller number of data than Model K. Model E with 18 components covers only slightly less data then Model D (by 0.2%), but the number of model-covered data drops with a further decrease of components (Model F, 15 components). Even less data are covered by Models I and L (86 and 85%, respectively), which have no first-order coefficients for major components. Model J, with an incomplete set of second-order coefficients (17 versus 36) and no first-order major coefficients, covers just 79% of the original data, whereas Model M with only 14 second-order coefficients, but a complete set of first-order major coefficients, covers 87% of the data.

As can be seen in Table 7, decreasing $\Delta^2$ by orders of magnitude (below the limit of genuine outliers) affects $n_s$ strongly by preferring data that accidentally happen to be close to calculated values. Note that the outcome of Models G and H, in terms of component coefficients, though fitted to only 53% and 21% of all data, is nearly identical to that of Model F, which represents 87% of all data.

## 6. Compensation effect, coefficient of determination, and *Others* component

The average activation energy, $B_a = n_s^{-1}\sum B$, where the summation is over all glasses on which the models is based, varies slightly from model to model (see Table 3) depending on which glasses were removed from the original database and which sets of viscosity-affecting components and their representation by first and second-order coefficients were chosen for different models. As Fig. 8 illustrates, the $A$ coefficient correlates neatly with $B_a$. This is a result of the compensation effect. By Eq. (1), each $B$ value is affected by $A$, and so is $B_a$ as the least-squares optimization adjusts $A$ to minimize the sum of $\Delta^2$ values. We would prefer to postulate that $A$ is a constant independent of glass composition. However, not knowing its correct value, we had no choice but to include $A$ as a fitting parameter and allow the least-squares optimization to determine its value. Disregarding Model J, the average value for all other models is $A = -11.36 \pm 0.10$, corresponding to $\eta_\infty = e^A = 1.17\times10^{-5}$ Pa·s.

Except for Models A and M, $R^2$ roughly correlates with $p$ (Fig. 9) for models with $\Delta^2 < 3.3\times10^5$ K$^2$. As expected, $R^2$ is higher, though only marginally, in Model A than in Model B (Table 3). Surprisingly, $R^2$ of Model M is nearly as high as that of Model D, even though it has much fewer second-order coefficients. In Models G and H, where $\Delta^2$ was low, $R^2$ was artificially increased without any difference in the model outcome.

*Others* coefficients are high in four models with no $B_i$s for major components (Models I, J, K, and L); see Table 3. This is a sign of a potential model uncertainty because the actual influence of *Others* depends on the *Others* composition, which is likely to vary from glass to glass, depending on the waste treated.

## 7. Deviation frequency distribution

To characterize the database, we used the relative deviation for viscosity, defined as $D = (\eta_M - \eta_C)/\eta_M$, where the subscripts $M$ and $C$ denote measured and calculated, respectively. After sorting data by $D$, from smallest to largest, we determined the deviation frequency to be $f_{100} = 100/(D_{100+i} - D_i)$, where $i = 1,2,\ldots, n_t - 100$ is the data sequence number and $n_t$ is the number of data points including outliers. The left panel of Fig. 10 shows the frequency for Model B plotted against $D$. The line represents the Gaussian distribution, $f_{100} = f_M \exp(-(D/D_0)^2)$ with $f_M = 12555$ and $D_0 = 0.284$ (fitted with the least-squares optimization; 57 data with $D > 0.685$ were excluded).

While most of the data are more or less randomly distributed, the number of outliers is higher than the normal distribution at approximately $-0.3 < D < 0.3$ would suggest, especially on the negative branch. Note that defining outliers as data for which the $\Delta^2$ exceeds a more or less arbitrary limit removes deviant data, as indicated in Fig. 1, but also omits low-probability data that are valid based on the normal (Gaussian) distribution. By setting $\Delta^2 = 3.3\times10^5$ K$^2$ as the acceptability limit, we attempted to remove data that do not

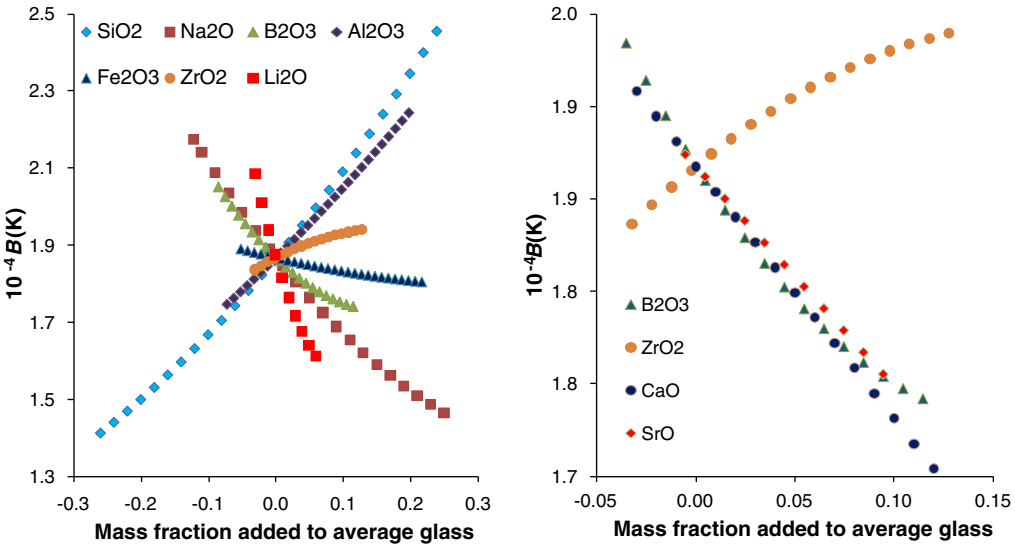


**Fig. 6.** Spider plot: effects of component additions to glass of average composition (Model F).

support the model. Apart from erroneous "bad" data, outliers include correct data located in highly nonlinear pockets of the composition region.

The right panel of Fig. 10 shows the frequency plotted against $D$ for Model D. The line represents the Gaussian distribution, $f_{100}$, with $f_M = 17517$ and $D_0 = 0.194$ (fitted with the least-squares optimization while 76 data with $D > 0.685$ were excluded). Here $f_M$ is higher than that for the first-order Model B and $D_0$ is smaller, both indicating a better fit of the second-order model. Interestingly, the two branches (negative and positive) of the distribution curve are not symmetrical, which is probably caused by fitting the model to $B$ rather than to $\eta$. The frequency of outliers is higher than the normal distribution at $-0.25 < D < 0.25$ would suggest. Such a fat-tailed distribution is encountered in economics (a source of underestimated risk). The fact that the number of outliers is higher in second-order Model D (76) than that in first-order Model B (57) indicates that most outliers were caused by measurement errors rather than the lack of fit. Measurement errors include volatilization, redox variations, crystallization and phase separation; errors in data recording and copying are also conceivable.

Fig. 11 compares calculated-versus-measured viscosity data of Models B and D. Interestingly, the first-order Model B underpredicted more data points than it overpredicted. The frequency of highly deviating data, Fig. 10, shows this in a different way.

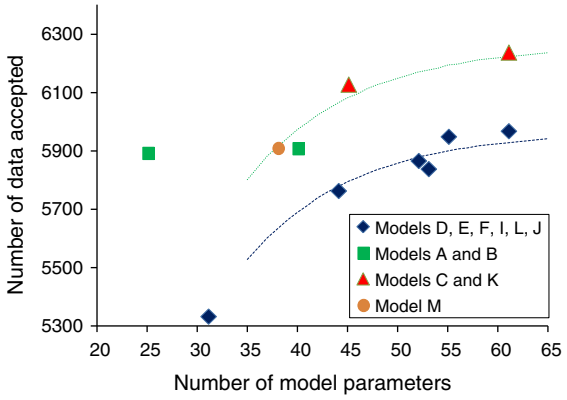


**Fig. 7.** Number of data accepted by model fitting versus model parameters.

## 8. Discussion

### 8.1. Effects of components and their interactions

Generally, the ionic charge, ionic radius, coordination number, etc., of glass constituents influence the macroscopic properties. However, attempts to correlate these properties, such as viscosity, with the atomic characteristic of glass components are only partially successful. Modeling the viscosity–composition function based on the "first principles" is unlikely to succeed until the actual molecular mechanism of viscous flow of multicomponent melts with complex component interactions is well understood. Component interactions have been discussed in the literature in terms of charge compensation effects, mixed-alkaline effect, association of species into larger structural units, etc. Our present work belongs to the category of empirical studies that provide data for glass structure researchers to match with theoretical predictions.

### 8.2. Model ranking

Models can be judged according to the number of data accepted by fitting the models ($n_s$), the number of components they cover ($N$), the number of parameters ($p$), the coefficient of determination ($R^2$), the value of the *Others* coefficient, etc. Another criterion is $D_0$, the width of the deviation frequency distribution. This we obtained for only two models (see Section 7) and it clearly favors the second-order model.

Models with high $n_s$, low $p$, high $R^2$, and a low $B_{\text{Others}}$ are generally preferable. Based on average ranking of models according to these four criteria, the models with $\Delta^2 < 3.3 \times 10^5$ K$^2$ (i.e., excluding Models G and H) rank, from highest to lowest, as M > E > D > C > A > F = B = K > J > L > I.

**Table 7**
Effect of $\Delta^2$ on data ranges and the number of data selected ($n_s$).

| Model | $\Delta^2$ (K$^2$) | $T_{\max}$ | $T_{\min}$ | $\eta_{\max}$ | $\eta_{\min}$ | $n_s$ | $\Delta n_s$ |
|---|---|---|---|---|---|---|---|
| F | $3.3\times10^5$ | 1747 | 800 | 375 | 0.27 | 5867 | |
| G | $3.3\times10^4$ | 1747 | 820 | 296 | 0.31 | 3589 | 2278 |
| H | $3.3\times10^3$ | 1503 | 850 | 200 | 0.51 | 1471 | 2118 |

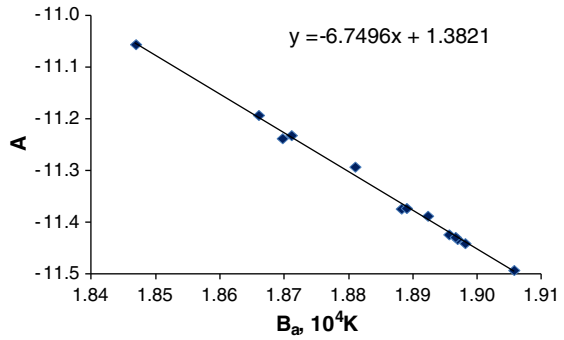


**Fig. 8.** Coefficient $A$ versus average activation energy.

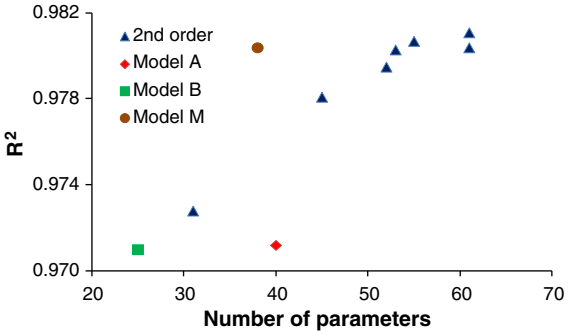


**Fig. 9.** Coefficient of determination ($R^2$) versus number of model parameters ($p$).

The high-ranking Model M keeps first-order coefficients of major components while using only selected second-order terms, thus affirming the common practice [13].

The ranking would change if different weights were ascribed to the evaluating criteria or additional criteria were used. Thus, Models C and K rank highest in $n_s$, Models B and J have the lowest $p$, Models D and E rank highest in $R^2$, and Model M has the lowest $B_{Others}$. On the other hand, Model J ranks worst in $n_s$, Models C and D have the highest $p$ (a disadvantage for some applications), Models A and B have the lowest $R^2$, and Model I has the highest $B_{Others}$.

Regardless of ranking, first-order models (Models A and B) are favored for their small number of parameters per component (1.0) and the ease of handling in applications, such as formulation of glasses with constrained properties using the matrix calculus. On the other hand, some second-order models may be selected because they cover a large number of compositions, or have high $R^2$, even though they have a high number of parameters per component (ranking from the lowest in Models J and M to the highest in Models E and F).

Some correlations mentioned in previous sections may bias the ranking. For example, low $R^2$ is generally associated with the lack of second-order terms (Models A, B, and J), the lack of first-order terms of major components (Models J, K, and L), a low number of parameters (Models B, J, A, L, and K), and a low number of components recognized as viscosity-influential (Models L and K).

Generally, models should be validated by data that were obtained independently of those used to fit the model equations. In this study, where we used a database containing thousands of data from multiple sources, the model is "validating itself" by the "law of large numbers".

## 9. Conclusions

The treasure trove of waste-glass property data compiled at PNNL [13] allowed us to perform numerical experiments with property-composition models in which we took advantage of the dependence of molten-glass viscosity on temperature via the activation energy

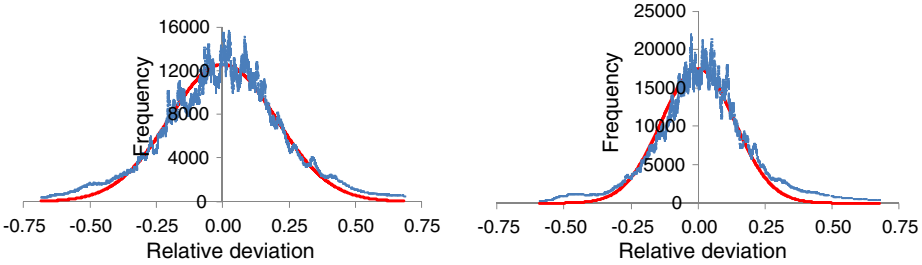


**Fig. 10.** Deviation frequency with Gaussian distribution line for Model B, left, and Model D, right.

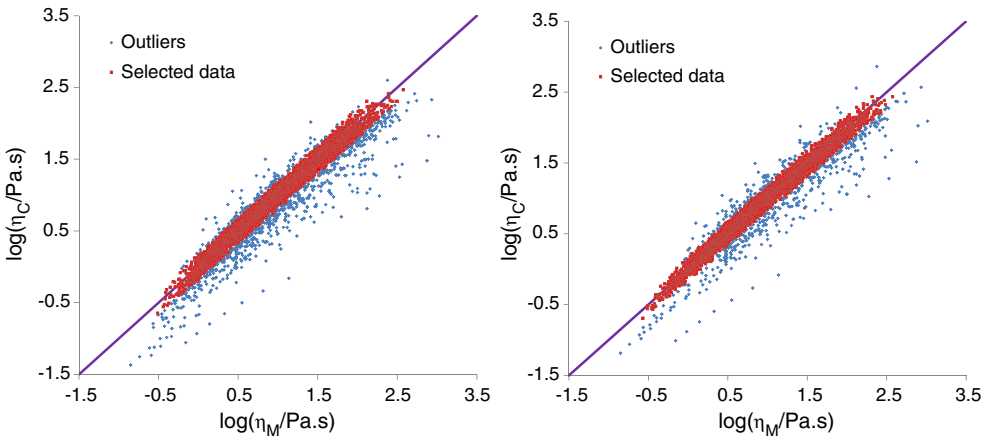


**Fig. 11.** Calculated versus measured values of log η (fitted to data points with $\Delta^2 < 3.3 \times 10^5$ K$^2$) for first-order Model B (left) and second-order Model D (right).

as a sole composition-affected parameter. The simplicity of computation made it possible to reduce arbitrariness in eliminating outliers, thus minimizing the difference between measured and calculated values for the maximum number of data. The outlier-free data exhibit a near-Gaussian distribution with respect to the frequency of the deviation between measured and calculated values.

Both first- and second-order models were developed for the original database, as well as several second-order models for a database from which extreme compositions were removed. Various sets of components were tested. Two first-order models, one for 39 and the other for 24 components, are easy to use in applications and represent the database with the smallest number of parameters per component. The second-order models have a higher number of parameters to represent binary interactions of major components, and consequently cover a larger database. The $R^2$ value was between 0.97 and 0.98 for all regular models.

The compensation effect between $A$ and $B$ in the Arrhenius Eq. (1) is evident even in the very large database and merits further study.

## Acknowledgements

This study was supported by a WCU (World Class University) program through the National Research Foundation of Korea funded by the Ministry of Education, Science and Technology (R31-30005). Financial support was also provided by the U.S. Department of Energy's Hanford Tank Waste Treatment and Immobilization Plant Federal Project Office, Engineering Division.

## References

[1] H. Scholtze, Glass—Nature Structure and Properties, Springer, New York, 1990.
[2] N.P. Bansal, R.H. Doremus, Handbook of Glass Properties, Academic Press, Orlando, 1986.
[3] SciGlass - Glass Property Information System, http://www.sciglass.info.
[4] A. Fluegel, Glass viscosity calculation based on a global statistical modelling approach," Proc. Eighth Advances in Fusion and Processing of Glass, Glass Technol.: Eur. J. Glass Sci. Technol. A 48 (February 2007) 13–30.
[5] A. Sipp, D.R. Neuville, P. Richet, Viscosity, configurational entropy and relaxation kinetics of borosilicate melts, J. Non-Cryst. Solids 211 (1997) 281–293.
[6] P. Hrma, High-temperature viscosity of commercial glasses, Ceramics-Silikaty 50 (2) (2006) 57–66.
[7] P. Hrma, Arrhenius model for high-temperature glass viscosity with a constant pre-exponential factor, J. Non-Cryst. Solids 354 (2008) 1962–1968.
[8] P. Hrma, Glass viscosity as a function of temperature and composition: a model based on Adam–Gibbs equation, J. Non-Cryst. Solids 354 (2008) 3389–3399.
[9] R.W. Douglas, The flow of glass, J. Soc. Glass Technol. 33 (1949) 120–162.
[10] J.C. Mauro, Y. Yue, A.J. Ellison, P.K. Gupta, D.C. Allan, Viscosity of glass-forming liquids, Proc. Natl. Acad. Sci. U. S. A. 106 (2009) 19780–19784.
[11] P. Hrma, B.M. Arrigoni, M.J. Schweiger, Viscosity of many-component glasses, J. Non-Cryst. Solids 355 (2009) 891–902.
[12] P. Hrma, Empirical models and thermodynamic constitutive functions for high-level waste glass properties, Ceram. Trans. 87 (1998) 245–252.
[13] J.D. Vienna, A. Fluegel, D.S. Kim, P. Hrma, Glass Property Data and Models for Estimating High-level Waste Glass Volume, PNNL-18501, Pacific Northwest National Laboratory, Richland, Washington, 2009.